Crystallization of GeO2 thin films into α-quartz: From spherulites to single crystals

Zhou, Silang; Antoja-Lleonart, Jordi; Nukala, Pavan; Ocelík, Václav; Lutjes, Nick R.; Noheda, Beatriz

Published in:
ArXiv

Document Version
Early version, also known as pre-print

Publication date:
2020

Citation for published version (APA):
Zhou, S., Antoja-Lleonart, J., Nukala, P., Ocelík, V., Lutjes, N. R., & Noheda, B. (2020). Crystallization of GeO2 thin films into α-quartz: From spherulites to single crystals. Manuscript submitted for publication.

Crystallization of GeO_2 thin films into *α-quartz*: from spherulites to single crystals

Silang Zhou[1,a)], Jordi Antoja-Lleonart[1], Pavan Nukala[1], Václav Ocelík[1], Nick R. Lutjes[1], Beatriz Noheda[1,b)]

[1)]Zernike Institute for Advanced Materials, University of Groningen, Nijenborgh 4, 9747AG
Gronignen, The Netherlands

Abstract

Piezoelectric quartz (SiO_2) crystals are widely used in industry as oscillators. As a natural mineral, quartz and its relevant silicates are also of interest of GeO_2 science and mineralogy. However, the nucleation and growth of quartz crystals is difficult to control and not fully understood. Here we report successful solid-state crystallization of thin film of amorphous GeO_2 into quartz on various substrates including Al_2O_3, $MgAl_2O_4$, MgO, $LaAlO_3$ and $SrTiO_3$. At relatively low annealing temperatures, the crystallization process is spherulitic: with fibers growing radially from the nucleation centers and the crystal lattice rotating along the growth direction with a linear dependence between the rotation angle and the distance to the core. For increasingly higher annealing temperatures, quartz crystals begin to form. The edges of the sample play an important role facilitating nucleation followed by growth sweeping inward until the whole film is crystallized. Control of the growth allows single crystalline quartz to be synthesized. Our study reveals the complexity of the nucleation and growth process of quartz and provides insight for further studies.

1. **Introduction**

Quartz (SiO_2) is one of the most abundant minerals in the earth's crust. It has been widely used in electronics as the key element in oscillator circuits. These oscillators use the mechanical resonance of a piezoelectric material to generate signals with a precise frequency, which requires high crystallinity of the piezoelectric. Quartz oscillators are found in computers, cellphones, wristwatches, clocks and radios[1]. The standard method of producing high quality quartz crystals is hydrothermal growth, followed by mechanical cutting and etching[2]. However, the size of the crystals made by this top-down method are limited to tens of micrometers, which in turn limits the frequencies to hundreds of MHz and it does not meet the high frequency current trends of information and communication technologies or the miniaturization trends in the microelectronic industry[3][4].

Recently, several reports have studied the synthesis of submicron-sized quartz, such as epitaxial quartz thin films on silicon by soft chemistry methods[5][6], homoepitaxy of quartz on quartz by ion beam implantation[7][8], hydrothermal growth of nano-quartz[9][10], as well as solvothermal synthesis[11] and microemulsion-mediated synthesis of quartz[12]. The challenge lies in the strong tendency of amorphization of silicon dioxide and the difficulty to control the nucleation and growth processes. It has been proved that the rigid network of SiO_4 tetrahedra makes the solid state transformation of silica into quartz impossible unless some catalyst ions, so-called 'network modifiers' or 'melting agents', are added[8][13]. These melting agents are usually alkaline metals or alkaline earth metals, well known in the glass industry to lower the melting points of silicates to a more accessible temperature. The network modifiers can form bonds with the oxygen atoms, breaking the connectivity between the SiO_4 tetrahedra and making the network less rigid. This leads to significant lowering of the melting points of the silicate and to an increased nucleation rate[14].

We have focused our study on quartz-type GeO_2[15][16]. At ambient conditions, the stable phase of GeO_2 is rutile and the quartz phase is meta-stable[16][17]. However, when pure GeO_2 is cooled down slowly from the melt, the quartz phase is formed instead and bulk single crystals of GeO_2 quartz can be stabilized up to 1000 ˚C[18], due to the extremely sluggish transformation from quartz to rutile[16]. Moreover, the melting point of GeO_2 is hundreds of degrees lower than that of SiO_2, due to the weaker bonds of Ge-O compared with those of Si-O[16]. The less rigid network of GeO_2 makes the solid-state crystallization possible without using melting agents.

We report successful solid-state crystallization of thin amorphous films of pure GeO_2 into the quartz structure by means of controlling the crystallization temperature. We have found that columnar and dendritic growth take place at high crystallization temperatures. If the crystallization temperature is lower, spherulitic crystallization is promoted due to high frequency of lattice defects formation. Spherulites are made of fibers that grow radially, staring from a nucleation core, conferring the typical spherical (or circular in two dimensions) shape to the spherulites. Spherulites are formed by non-crystallographic branching, where the parent and daughter fiber do not share the same crystal orientation, with misorientation angles that can range between 0-15 ˚[19]. Using local crystal orientation inspection, we have characterized the lattice rotation along the fibers' growth directions. The formation of spherulites from the liquid phase requires high crystallization driving force, usually provided by high supersaturation or supercooling and spherulites can be found in different kinds of materials such as polymers[20], small molecules[21] or inorganic minerals[22]. In nature, spherulitic forms of quartz, such as chalcedony[23], and other silicates can be found in volcanic rocks. However, to our knowledge, spherulitic crystallization of pure quartz from amorphous solid has never been discussed in the literature. Most of the studies on spherulites are focused on polymers, which often have complex structures with folded chains. Our simple system may shed light upon the spherulitic growth process and its control.

2. Experimental

Thin amorphous films of GeO_2, with thicknesses of about 100 nm, were deposited by pulsed laser deposition (PLD) using a 248 nm KrF laser (Lambda Physik COMPex Pro 205). The target was made from cold pressing of GeO_2 (Alfa Aesar, 99.9999 %) powders. In some cases, a TiO_2 buffer layer was deposited. For that purpose, pellets were made using TiO_2 powders (Alfa Aesar, 99.6 %). The substrates used were: Sapphire Al_2O_3 (0001), *MgO* (110), Spinel $MgAl_2O_4$ (110), $SrTiO_3$ (*STO*) (001), *Nb*-doped $SrTiO_3$ (*Nb-STO*) (001), $LaAlO_3$ (*LAO*) (001) (CrysTec GmbH). Since the nucleation was found to happen at the edge of the sample, the size of the substrate influences the process. In our experiments, the size of the *LAO*, *STO*, *Nb-STO* substrates were 5 × 5 mm^2; $MgAl_2O_4$, *MgO* and Al_2O_3 were mechanically cut from 10 × 10 mm^2 piece to be also approximately 5 × 5 mm^2. The substrates were glued with silver paste on a heating plate, which was heated from the back with a laser (DILAS Compact-Evolution, wavelength 808 nm).

The deposition parameters of the GeO_2 (TiO_2) growth were optimized at a target-substrate distance of 46 mm (52 mm), a fluence between 2.5 -3.5 J/cm^2 (~2 J/cm^2), deposition temperature of 600 ˚C (600 ˚C), oxygen pressure of 0.1 mbar (0.1 mbar) and a laser repetition rate of 5 Hz (1 Hz). After the deposition, the GeO_2 thin films are amorphous and annealing is necessary for crystallization. The films were annealed at 830 ˚C*,* 880 ˚C *or* 930 ˚C (*a*s described later), with an oxygen pressure of 200 mbar for 30 minutes. Subsequently, the films were cooled down to room temperature with a rate -5 ˚C*/*min.

The local crystallinity and crystal orientations were characterized by Electron Back-Scatter Diffraction (EBSD), performed on a FEI Nova NanoSEM 650 scanning electron microscope. The sample was pre-tilted on a 71 ˚ holder. Thin films grown on *Nb-STO* (conducting) substrates were observed in high vacuum with a standard secondary electron detector. Films grown on the other (insulating) substrates, were measured in 0.5 mbar of chamber pressure with a Low Vacuum Detector to minimize charging effects. EBSD data was collected in both cases using an EDAX EBSD system equipped with a Hikari CCD camera for recording Kikuchi patterns, with speed between 5-20 p/s and distances between neighbor points from 0.15 to 1 *µm,* at 20 keV of acceleration voltage and about 10 nA of current in the primary electron beam. EDAX OIM Analysis 8.1 and Matlab® based toolbox MTEX[24] software were used for EBSD data analysis. Inverse Pole Figure (IPF) and Image Quality (IQ) maps were plotted along three axes [100], [010], [001] in Cartesian coordinates, where [001] is the out-of-plane direction of the sample and [100] and [010] are in-plane directions, [100] direction being horizontal on the maps. The average crystallinity was checked by X-Ray Diffraction (Panalytical X'Pert, CuK_α *ra*diation) and the morphology was imaged by Atomic Force Microscope (AFM) (Bruker Dimension Icon). Local structures were further characterized by atomic resolution High Angle Annular Dark Field Scanning Transmission Electron Microscopy (HAADF-STEM) measurements using a Themis-G, double corrected electron microscope at 300 kV. Cross-sectional lamellae for STEM analysis were prepared via Focused Ion Beam (FIB, Helios 660) based procedure.

3. **Results**

3.1. Crystallization of GeO_2 on Al_2O_3(0001) substrates

Figure1 shows the crystallization of GeO_2 into quartz on sapphire (Al_2O_3) *s*ubstrates at different annealing temperatures. Films grown on these substrates are only partially crystallized and a significant volume of the material remains amorphous. When the films are annealed at 830 ˚C*,* dense and compact spherulites with diameter of around 50-100 *µm a*re formed, as shown in Figure1a)-b). As mentioned in the introduction, these spherulites are spherical (or circular) structures that consist of fibers growing radially and quasi-isotropically from a single nucleation point. The different colors in the Inverse Pole Figure (IPF) maps indicate the different orientations of the fibers. The black lines in the maps of Figure1a) (and in the rest of this work) denote the boundaries between neighboring fibers that present differences in the orientation angles larger than 3 ˚*.* We denote these regions delimited by the solid lines as "grains" for the sake of the discussion. However, each such spherulitic grain is composed of many fibers as shown in figure S1 (see Supplementary Information). Within one grain, changes in orientation are visible. It can be observed that, while in the two smaller spherulites of Figure1a) and c), most of the fibers belong to the same grain (most fibers are misoriented by less than 3 ˚ with respect to their neighbors), for the big spherulites, which have nucleated from a contamination particle, many more grains are present. Statistical analysis of the misorientation angle distributions of the EBSD maps (see figure S2 in Supplementary information) also shows that almost 80 *%* of the observed misorientation angles between neighboring grains in the same spherulite are within 5 ˚. This small angle branching is the characteristic behavior of spherulitic growth[19].

The morphology of such spherulites is also characterized by SEM (Figure1b)) and AFM (see figure S1 in Supplementary Information). The AFM images reveal a protruding core of about 500 nm in diameter at the center of the spherulite, serving as a nucleation center. Fibrils grow radially from the core. It is also visible that the spherulites are lower in height compared to the amorphous surroundings, as expected due to densification upon crystallization.

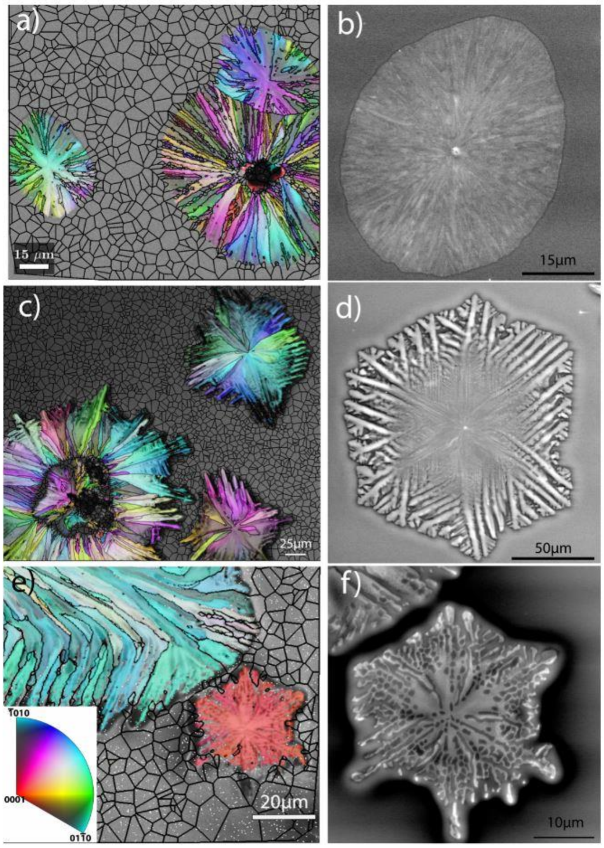

Figure 1. EBSD (left) and SEM (right) images of quartz crystals on Al_2O_3 substrates crystallized with different annealing temperature, showing different crystallization features: a)-b) The films annealed at 830 ˚C show typical spherulites with dense radially-grown fibrils. c)-d) films annealed at 880 ˚C show spherulites with dendritic growth at the spherulite edge. e)-f) thin films annealed at 930 ˚C show single crystalline growth. a), c), e) images are made by overlaying the Inverse Pole Figure (IPF) color map and the Image Quality (IQ) b&w map viewed along the out-of-plane [001] direction of the sample, in which the black lines indicate the grain boundaries with misorientation larger than 3 ˚. e) and f) are taken at the same sample area. Inset in e) shows the color legend for all three IPFs.

As shown in Figure1c) and d), increasing the annealing temperature promotes a more anisotropic growth, with fingering patterns at their growth fronts and the shape of some crystals reflecting the symmetry of quartz ($P3_221$ or $P3_121$)[25]. It can be observed how the number of grains decreases dramatically compared to those at the lower temperature growth, leaving only few of them with exaggerated aspect ratio. As shown from the SEM image (Figure1d)) and AFM (see figure S1 in Supplementary Information), the center of the spherulite is flat with a core in the middle, and it develops a hexagonal shape, reflecting the symmetry of the (0001) plane of quartz. At some distance from the core, it branches into bundles of fine fibers forming a rougher structure. Fractal growth of daughter fibrils protruding also at specific angles with respect to the parent ones fills the space.

If the annealing temperature is increased further to 930 ˚C, single-crystal quartz domains are formed as shown on the right side of the EBSD map in Figure 1e) and as a magnified SEM image in 1f). The homogeneous red color of the crystal in the [001] IPF map indicates that the c-axis of the crystal points out of surface plane, and its hexagonal shape reflecting the symmetry of the quartz in that orientation. AFM scans (figure S1 in supplementary Information) show no fibrous growth, suggesting a different crystallization mechanism.

Moreover, some bumps about 200 nm in diameter which give dark contrast in the SEM image appear, which suggests they may be porous amorphous material which has not crystallized yet.

As mentioned above, Figure1a), c) shows that in each grain which is composed of fibers, whose local crystal direction is changed gradually as the fiber grows. A quantitative analysis reveals that the quartz lattice rotates linearly along the fiber growth direction, as shown in the example of Figure2. The point-to-origin crystal rotation angle increases linearly along the fiber with an average slope of 1.25 ˚/*µm.* In addition, the point-to-point misorientation angle value along the same line does not exceed 2 ˚ (distance between scanning points is 0.4 *µm*)*,* which explains why the selected fiber is contained in one grain, despite the large misorientation that exists between its beginning and its end (35 ˚)*.*

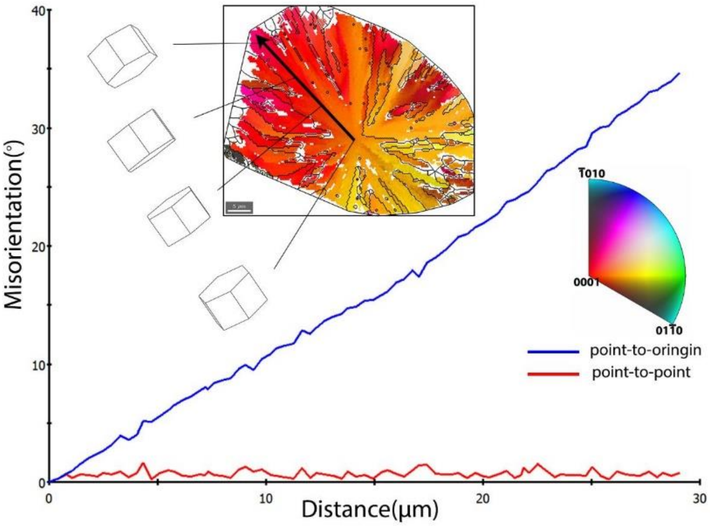

Figure 2. Lattice rotation inside one fiber of a spherulite formed during crystallization at 830 ˚C on Al_2O_3 substrates. Lattice rotation is expressed in the form of point-to-origin crystal misorientation angles as a function of distance along the fiber starting from the center towards the edge of the spherulite. The inset represents the [110] IPF map of the spherulite, with the black arrow indicating the measurement direction. The local rotation along the fiber is visualized by means of quartz crystal shapes, viewed along [001] direction, at four different points along the black arrow.

This kind of rotating lattice has been previously observed in similar amorphous to crystalline solid transformation (e.g. in Fe_2O_3[26] or $Sb_{3.6}Te$[27] by *in situ* electron beam annealing in TEM, or on Sb_2S_3[28] by laser surface annealing). Savytskii et al., suggest that the lattice rotation is accompanied by re-arrangements of dislocations and conclude that unpaired dislocations, caused by the stress generated from the volume change during crystallization, are the origin of the continuous lattice rotation[28]. Single quartz grain rotation during its growth from thin amorphous layers deserves a separate study, which will be the subject of future work.

Interestingly, the typical crystal rotation gradient inside a fiber of the spherulites annealed at 830 ˚C *is* about 0.5-1.5 ˚/*µm,* while for those annealed at 880 ˚C*, t*he rotation rate decreased to about 0.25-0.5 ˚/*µm,* being absent for the single crystals formed during annealing at 930 ˚C*.* The decreased lattice rotation with increasing annealing temperature may be associated to a smaller stress due to the smaller volume change taking place at higher temperature, accompanied by a higher dislocations mobility. Since reported spherulitic lattice rotation happens in solid-to-solid, amorphous-to-crystalline transformation, we propose that the single crystal domain formed during annealing at 930˚C are nucleated from, or close to, the liquid phase.

Besides the spherulites and single crystals that are grown from a single nucleation point described above, the largest crystallized areas belong to crystals that nucleate from the edge of the sample and sweep inwards (see green area in Figure1e)). As shown in the supplementary information (figure S3), a line of half spherulites are formed at the edge of the sample, which shows the strong preference for nucleation at the sample edge. Some of their fibers grow beyond the circular peripheries of the spherulites, resulting in a continuous spherulites area occupying most of the crystallized area. From now on, we will call the spherulites grown from single nucleation point, as those shown in Figure1, single-nucleus spherulites, to distinguish them from the continuous spherulites regions, which are an assembly of fibers grown from multiple nuclei and usually starting from the edge of the sample.

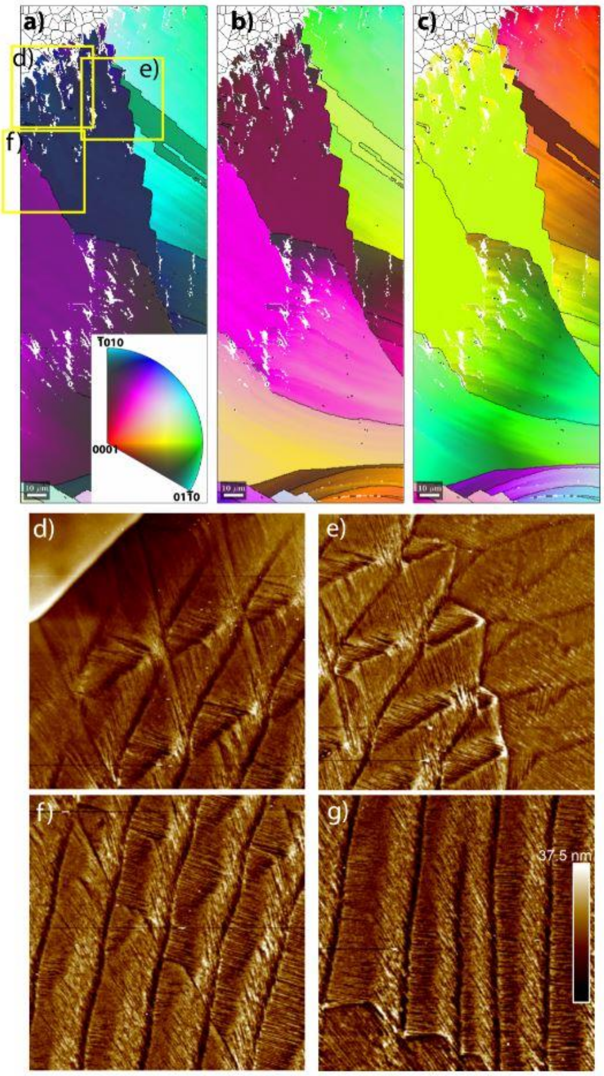

Figure 3. Continuous spherulites grown from the sample edge on Al_2O_3 substrate annealed at 830 ˚C. a)-c) IPF map viewed along [100], [010] and [001] directions, respectively. (scans were taken from the area in the black rectangle in S4). d)-f) AFM scans at the place indicated by the corresponding yellow squares in a) show fibrous growth with periodic modulations in height, reflecting in each case, two superimposed growth wave fronts. g) AFM scan at a different location in figure S4 (see Supplementary Information). The scale bar at g) serves for all AFM scans.

Figure3 shows these larger Continuous spherulites of a film annealed at 830 ˚C. At this relatively low temperature, these crystalline areas also show spherulitic growth with needle-like fibers growing from the sample edge and forming a circular and smooth growth front. Lattice rotation can also be clearly observed in some of the grains as indicated by their color gradients, while for other grains there is almost no lattice orientation change. Interestingly, two types of modulations of the surface are detected by AFM in a few locations marked on Figure3a): large concentric surface waves and a multitude of tiny trenches coexist in those regions as shown in Figure3d)-g). The quasi-periodic waves that modulate the surface morphology and the interference between two modulation fronts is clearly captured in Figure3d)-g).

In these images, the continuous concentric shape of one growing front is deformed by a neighboring one that remains concentric (see Figure3d)-g)), indicating that the growth fronts were not formed at the same time (the non-deformed one is formed after). This also seems to indicate that the waves, giving rise to the large surface steps, are not formed during the crystallization process, but during the cooling down process, when internal stress accumulated due to a difference in thermal expansion coefficient between GeO_2 quartz and the substrate. The stress is relieved subsequently by local slip in two slip planes with local maximal shear stress components. On the other side, the system of dense trenches or tiny surface steps observed in Figure3d)-g) is probably formed immediately after or during crystallization. The fact that these trenches are only detected in fiber areas without lattice rotation suggests that the strain that arose during crystallization in these areas is not used to locally bend the crystal, but instead it is relieved by dislocation movement along appropriate slip planes, forming the tiny steps at the surface.

Figure4 shows one of the continuous spherulites for the films annealed at 880 ˚C. *T*hese crystals show preferred orientation with $(10\bar{1}0)$ *ou*t-of-plane and [0001] *di*rection parallel to [001] *sa*mple direction. The pole figure in Figure3d)-e) attests to the strong texture of the film. This orientation is the same as that of epitaxial thin films of quartz (SiO_2) grown on silicon[5], which was attributed it to the lattice match with the silicon substrate. In our study, the substrate is sapphire (0001), which has a hexagonal in-plane lattice with a= 4.758 Å, c= 12.988 Å[29] while the lattice parameter for bulk GeO_2 is a= 4.984 Å, c= 5.647 Å[15]. This does not offer a good lattice matching, being the smallest lattice mismatch 4.54 *%* along the $[11\bar{2}0]$ direction. Our finding suggests that $(10\bar{1}0)$ *ma*y be an energy-favorable plane, or at least kinetically favored with thin film crystallization at this temperature, independently of the epitaxial relations.

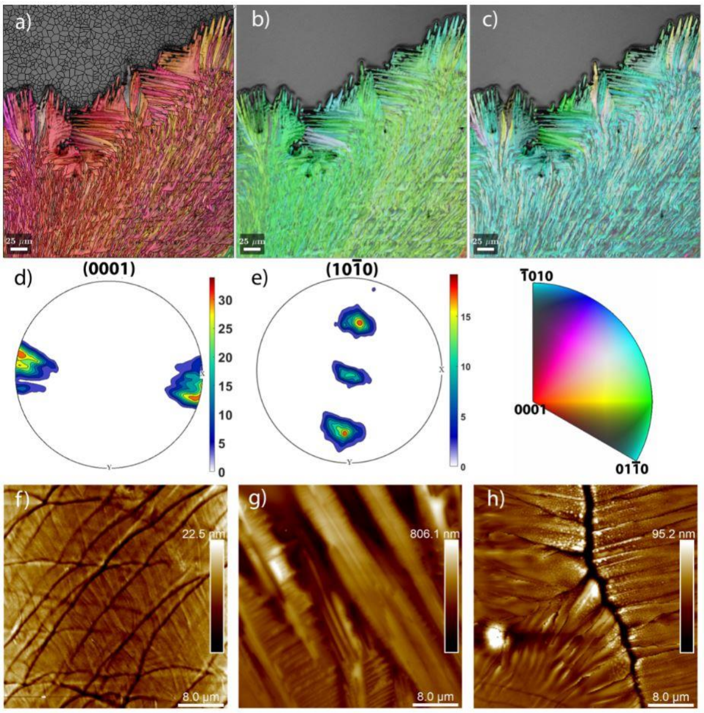

Figure 4. Quartz crystals grown from the sample edge on Al_2O_3 substrates annealed at 880 C˚ show spherulitic growth at the beginning (closer to the bottom edge) but with columnar-dentritic growth at the growth front. a)-c) [100], [010] and [001] IPF maps, respectively, with near uniform color suggest the preferred $(10\bar{1}0)$ out-of-plane orientation. d)-e) Pole figures of this area showing the strong texture. f) AFM image of the spherulitic growth with the waves imposed on the fibers. g) AFM image of the dendritic growth front and the depletion region around it. h) AFM image of two growth fronts meeting with each other and the boundary between them.

From the observation of grain boundaries (solid lines in the Figure4a)), it is obvious that the initial stages of the growth close to the edge nuclei, the growth is spherulitic, with the structures composed by many fibers; while at the growth front, the grains are differently oriented resembling columnar growth. The grain boundaries in Fig.4a) indicate that these columns are just continuation of the fibers, but in different direction. The majority of these columns have their longitudinal, e.g. growing axis, well aligned with [0001] *cr*ystal direction.

Figure4f) shows the morphology of a typical area of the spherulitic part, where fibers can be clearly observed. These fibers are thicker than those of film annealed at 830 ˚C and two sets of waves intercept with them, but they are less organized compared to the waves in Figure3d)-g). As mentioned above, at the growth front, oriented crystals with dendrite-like structures are found, similar to those in the single-nucleus spherulites. AFM scans (Figure4g)) show that the crystalline dendrites can be as high as 800 nm. Considering the thin film is only about 100 nm thick, a large mass of the material has migrated to the growth front to form these fingers, resulting in the depletion region around the fingers, which may prevent further growth.

At the growth front, lattice rotation is also observed at this higher temperature with a rate of about 0.2-0.6 ˚/*μm,* which is similar to that of the single-nucleus spherulites described earlier. On the other hand, inside the spherulitic region, the surface modulations modify the morphology as shown in Figure4f), giving rise to short and curved fibers, which makes the measurements more difficult than at the growth fronts. Further analysis shows that for some fibers, there is a linear lattice rotation while for other fibers, there is lattice change along the growth direction without clear relationship.

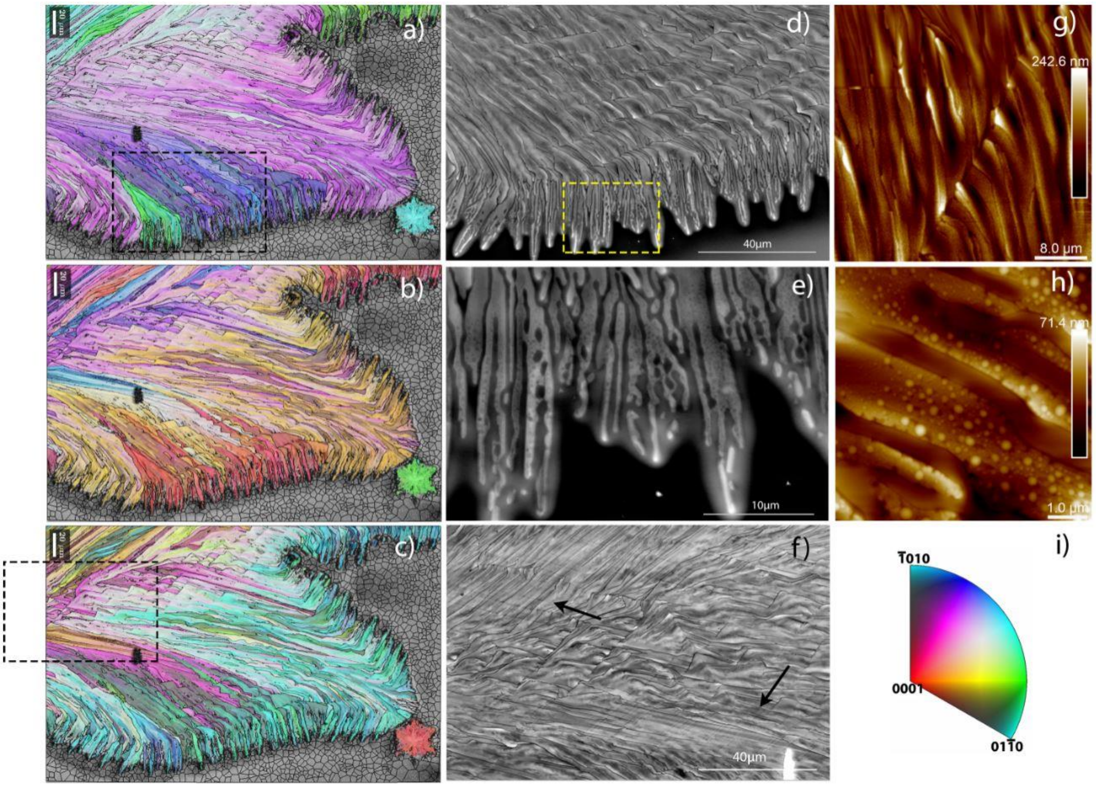

Figure 5 Quartz crystals grown from the sample edge on Al_2O_3 substrates annealed at 930 ˚C. a)-c) Overlay of IPF and IQ maps viewed from [100], [010] and [001] directions, respectively. d) SEM picture of the area in the black rectangle in a) showing the fibrous growth. e) zoom in of the yellow rectangle in d) shows the morphology at the growth front. f) SEM picture of the area in the black rectangle in c) and the black arrows point out the slip regions with groups of parallel lines on the film. g) AFM scan of the spherulitic area. h) AFM scan of the growth front with tall columnar features meeting with each other. i) color legend for a)-c).

Figure5 shows the crystallization of the edge-nucleated crystals with a still higher annealing temperature of 930 ˚C. It is shown that the fibers nucleate from the left part of the figure and they grow radially and keep branching till they reach the growth front, where the growth transforms into dendritic again. Interestingly, while the fibers started with a large variety of orientations, the dendrites at the growth front are also preferably oriented with the $(10\bar{1}0)$ again out-of-plane, as shown in Figure5c). Moreover, a close look of the in-plane directions (Figure5a)-b)) shows that the c-axis [0001] of the crystal lies along the long axis of the columns (the fastest growth direction) which is similar to the growth fronts with annealing temperature 880 ˚C as shown in Figure4. Therefore, fibers with the original orientation different than the preferred orientation lose in the competition, stopping the growth before reaching the growth front.

Generally speaking, the linear lattice rotation does not hold anymore in this case for both the spherulitic and the columnar growth. For some fibers, linear lattice rotation does happen but, in most cases, the fibers are not rotating at all or just change the orientation without a general trend.

Figure5d) shows the morphology of the area in the black rectangle in Figure5a) in which the growth, branching of the fibers and the interaction with the waves are clearly captured and it can be observed that these columns are continua of the spherulitic fibers. At the columnar growth front, as shown in Figure5e), there are a number of small dots which produce dark contrast in the image. AFM images scanned at the growth front, as shown in Figure5h), reveal that these small dots are protuberances of about 200 nm in diameter and 10 nm in height, similar to what was observed in single nucleus crystals (Figure1f) and figure S1), suggesting they may have similar growth mechanism. Figure5f) is the SEM image corresponding to the area in the black rectangle in Figure5c). Groups of parallel lines (also observed in figure S5) which are the slip traces[30][31], appear. Interestingly, at the places where slip occurs, the fibers are straight and no waves appear.

It should be noted that with the 930 ˚C annealing temperature, the film shows signs of melting and evaporation, with some parts of the sample in which GeO_x coalesces to form droplets, revealing the bare Al_2O_3 substrate. Similarly, to crystallization, amorphization also starts from the edge (see figure S6 in Supplementary information). The melting point of bulk GeO_2 is about 1100˚C[16] but our work suggests the surface energy can lower this considerably.

3.2. Crystallization of GeO_2 on MgO (110)

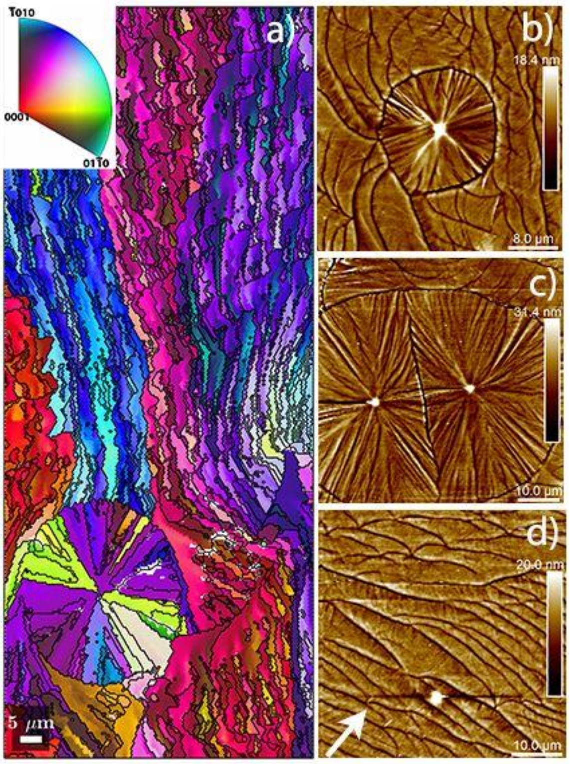

Figure 6 Complete crystallization of GeO_2 on MgO substrates annealed at 830 C˚: a)[100] IPF Map of an area with full crystallization showing one circular spherulite embedded in the matrix of wave-like spherulites starting from the sample edge. b)-d) AFM images of different areas of the sample. White arrow in d) points to the growth direction.

The crystallization on MgO substrates is shown in Figure6, where small circular single nucleus spherulites with dense fibers are embedded in a matrix of the huge edge-nucleated spherulites. Unlike for the growth on Al_2O_3, the entire film is successfully crystallized into quartz after annealing, which indicates that the nucleation and growth are facilitated on MgO. Figure6b)-d) shows the typical growth morphologies of quartz crystals on MgO which, otherwise, are similar to the morphologies on Al_2O_3: preferred nucleation at the edges with fibers growing radially and propagation of mass with wave fronts perpendicular to the growth directions, coexisting with a smaller number or isotropically grown single nucleus spherulites that nucleate in the center of the films.

3.3. Crystallization of GeO_2 on $MgAl_2O_4$(110) substrates

Figure7a) shows the crystallization of GeO_2 on $MgAl_2O_4$(110) substrates with annealing temperature of 830 ˚C. It can be observed that the films are only partially crystallized in the form of quasi-circular spherulites and a significant volume ratio of amorphous material is still present. The growth is not fully isotropic with grains with larger aspect ratio growing radially, similar to the features seen on sapphire for a higher annealing temperature of 880˚C. The image analysis shows that the central area of every spherulites has a relatively homogeneous orientation and, upon further growth, it branches into larger features with various orientations. The orientation of the different spherulites centers varies indicating no preferred orientation of nucleation, similar to what is observed on the sapphire and MgO substrates.

The morphology of such spherulites is also characterized by AFM, as shown in Figure7b)-c). In the center of the spherulite, the protruding core of about 500 nm in diameter serves as a nucleation center. Radial fibrils start growing from this core until it begins to branch into dendritic features to form rougher structures, being the central area of the spherulite significantly flatter than the edges. A closer view on the edge of the spherulite in (Figure7c)) shows that these areas are composed of bundles of fine fibrils.

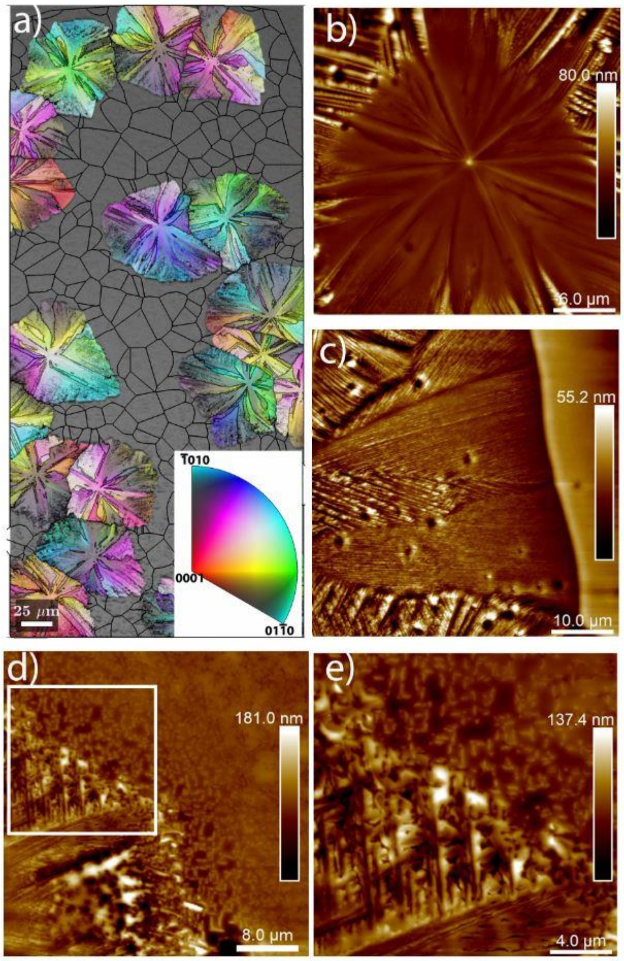

Figure 7 Quartz spherulites on $MgAl_2O_4$ substrates annealed at 830 ˚C: a)-c) and 880 ˚C: d)-e). a) [001] IPF map of quartz single-nucleus spherulites surrounded by amorphous GeO_2 (grey area). b) AFM scan of the central part of a spherulite. c) AFM scan of the bundles of fine fibers at the peripheries and smooth boundary. d) AFM image of the boundary shows a large number of rods formed in the amorphous area. e) Blow-up of the white square in d)

When the annealing temperature is increased to 880 ˚C*, t*he number of spherulites increases significantly (see figure S7) and the morphology changes, as shown in Figure 7d)-e): the spherulite boundaries are not smooth anymore and the growth front shows clear fractal growth where sub-individual dendrites grow out of the parent branches with an angle of 60˚. Interestingly, crystal rods with length about 1 μm *a*nd width about 200 nm appear at the amorphous area. The closer to the spherulite, the higher they are. Concomitant with the increase in height of these rods, the neighboring trenches also become deeper, which suggests they may provide the material for the formation of the rods. Traces of these rods are also found in thin films annealed at 830˚C*, a*lthough they are less noticeable.

From all the substrates we have used, only on $MgAl_2O_4$ *th*ere is no preferred nucleation at edge of the sample. As can be observed from figure S7, a cluster of spherulites appear very close to the sample edge and on the contrary, there is only one spherulite with its nucleus exactly on the edge. Moreover, the features of the rods are also only observed on $MgAl_2O_4$. This suggests the nucleation and growth process on $MgAl_2O_4$ *ha*ppens through a different mechanism.

3.4. Crystallization of GeO_2 on *LAO* and *STO* (perovskite) substrates and the formation of $SrGe_{3.3}O_{5.6}$

For films grown on $SrTiO_3$(*STO*) and *Nb*-doped $SrTiO_3$(*Nb-STO*) substrates, with an annealing temperature 830˚C*, t*he morphology and crystallinity are almost the same. It is easier to do EBSD and obtain better resolution of electron microscopy on *Nb-STO*, due to its conductance. The first feature to be noticed is that, already under the optical microscope, the thin films are covered completely by colorful crystals (see Figure S8). A SEM image in Figure8a) shows these crystals, of about 200*µm i*n diameter, have a typical spherulitic morphology. To one's surprise, EBSD shows the film is composed of long fibers (see Figure S8), and it does not correspond to the morphology of the spherulites in Figure8. Further investigation reveals that the spherulites in Figure8a) are not made of quartz but a germanium oxide with *Sr* in it, with the quartz layer being crystallized on top it. Because GeO_2 quartz and amorphous GeO_x *ar*e both transparent, the optical microscope only shows the germanium strontium oxide below the quartz, as observed in Figure8a). supplementary figure S8 clearly shows the difference between the quartz GeO_2 and amorphous GeO_x *on* top of the germanium oxide with *Sr*.

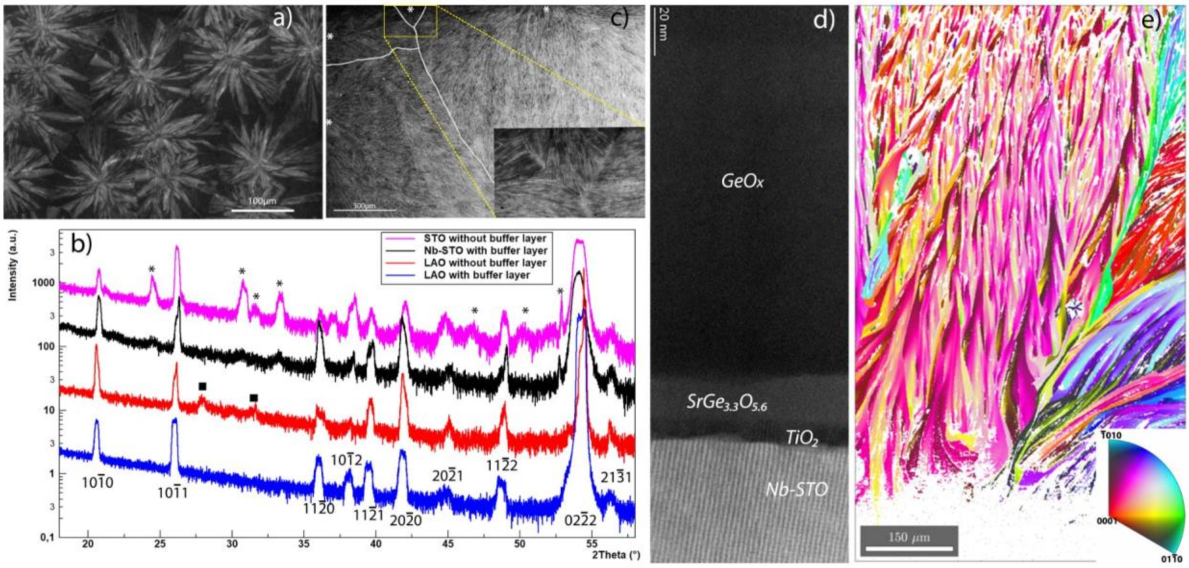

Figure 8 a) SEM image of GeO_2 on *Nb-STO* without using TiO_2 buffer layer. It shows the under layer of groups of spherulites which turn out to be $SrGe_{3.3}O_{5.6}$. The top layer quartz is not clear visible due to lower contrast. b) XRD patterns of thin films grown on *STO* and *LAO* with and without a *TiO2* buffer layer. Star and square marks the peak which cannot be assigned for quartz. c) SEM image of GeO_2 on *Nb-STO* with a TiO_2 buffer layer shows the film is composed of huge quartz spherulites with nuclei on the edge of the sample. White start marks the nuclei at the edge of the sample and white lines represent the boundaries between the spherulites. The inset is the blow-up for the yellow rectangle. d) HAADF-STEM image of the cross section of GeO_x on *Nb-STO* without using TiO_2 buffer layer showing the complexity of the film due to the interfacial reaction between GeO_x and *Sr*, resulting in the formation of a germanate. e) IPF of GeO_2 grow directly on *LAO* without TiO_2 viewed along [010] direction. All the samples here are annealed at 830˚C

As shown in the XRD pattern in Figure8b), besides the set of diffraction peaks characteristic of quartz GeO_2, additional peaks marked by the star symbol may be attributed to these spherulites. To understand what is going on, a cross-section of the sample was studied by Transmission Electron Microscopy (TEM) as shown in Figure8d). These experiments show that the situation is somewhat more complex: from the elemental analysis we learn that the Sr atoms of the STO substrates diffuse and react with the GeO_x *de*posited on top, forming a new compound. Using Energy Dispersive X-ray Spectroscopy (EDS), we estimate the chemical formula for this new compound to be $SrGe_{3.3}O_{5.6}$, which, to the best of our knowledge, has never been reported before.

With the *Sr* diffusing out of the *STO* lattice, it leaves behind protrusions of TiO_2 and *Ti*-rich *STO*. The TiO_2 protrusions are in the anatase phase and have perfect epitaxial relationship with the *STO* substrate. Some *Ge* also diffuses into the TiO_2 and forms *Ge*-doped TiO_2 regions. Since *Sr* is a network modifier used in the glass industry[14] and it is also used in thin film as catalysis to help crystallizing quartz[5], it is of no surprise that it will react with GeO_x at this temperature. On the contrary, according to Dietzel's field strength theory[14] , small cations with high charge favor the formation of glass and *Ti* is classified as "intermediate" (not a modifier). Only part of the GeO_x layer is transformed into $SrGe_{3.3}O_{5.6}$, which suggests there could be a blocking effect by the TiO_2 layer for the supply of the Sr into the GeO_x layer (see supplementary figure S9).

To test this hypothesis, another layer of TiO_2 was deposited on *Nb-STO* as a buffer layer. RHEED shows the TiO_2 layer has grown epitaxially on *STO* substrates (see supplementary Figure S9). After the growth of the buffer layer, a layer of GeO_2 was grown with the same recipe used for the films grown directly on the substrates. For films grown on *Nb-STO* with TiO_2 buffer layer, a direct inspection under the optical microscope shows that the colorful spherulites are gone, as shown in Figure S10 and the entire film is crystallized. However, from the XRD pattern, a trace of the $SrGe_{3.3}O_{5.6}$ can still be found.

Figure8c) shows the morphology of the film of GeO_2 on TiO_2-buffered *Nb-STO* substrate. Interestingly, the whole film is composed of several huge spherulites with nuclei locate at the edge of the sample, as marked by the white stars in the figure, and all the fibers can be tracked back to one of these nuclei. It is clear that the fibers grow radially and keep branching until they meet the fibers from the neighboring spherulites. The white lines in Figure8c) represent the boundaries between the spherulites. It can be seen that the small spherulite in the yellow rectangle lost in the competition of growth and there is no room for its further growth, similar to what is observed on other substrates. However, unlike on other substrates, single-nucleus spherulites are not observed at the sample center. Thus, we can conclude that the growth rate on TiO_2-buffered *STO* is accelerated significantly: once one nucleus is formed at the edge, it grows so quickly that a large part of the surface is covered before other nuclei can form.

To study the influence of TiO_2, thin films of GeO_2 were also deposited on another perovskite substrate, i.e. *LAO*, with and without TiO_2-buffer layer. For both cases, the film is fully crystallized using the same annealing temperature of *STO* and XRD patterns are also similar, except that the sample without TiO_2-buffer layer has small extra peaks, marked in black square in Figure8, which could not be assigned to quartz. Both films show similar spherulitic growth. Under the optical microscope, the morphology of the thin films on *LAO* with buffer layer is similar to the thin films on *STO* with buffer layer (See figure S10 in Supplementary Information). Figure8e) is the IPF Map of such a GeO_2 film directly grown on a *LAO* substrate which shows typical spherulitic growth.

4. **Discussion**

Although observations and modelling of spherulites have been reported extensively, the underlying mechanisms are still under investigation. Spherulitic-to-single crystalline transformation upon decreasing undercooling (increasing temperature) is a general trend for spherulites. Similar observation has also been found on 1,3,5-Tri-a-Naphthylbenzene[32], hippuric acid and tetraphenyl lead spherulites[33]. One possible origin for this transformation in our films could be the different ratios of rotational D_{rot} to translational D_{tr} diffusion coefficients at different temperatures[34]. When the temperature is high, both D_{rot} and D_{tr} are large, and the material attached on the growth front is able to align itself to follow the orientation of the growth front. If upon decreasing temperature, D_{rot} decreases more sharply than D_{tr}, the material attached on the growth front may be kinetically trapped in a relative minimum, misoriented with respect to the growth front. For the spherulites such as those in Figure1d), the edges show dendritic crystallization. Transitions from spherulitic to dendritic growth are expected with increasing temperature or/and decreasing supersaturation[34]. For example, Magill and Plazek showed that when the single crystal of 1,3,5-Tri-a-Naphthylbenzene is down-quenched to low temperature, its growth front starts to branch into small fibers and finally takes on spherulitic morphology. On the contrary, if this spherulite is up-quenched back to high temperature, the growth is shifted back to single-crystalline growth[32]. So one explanation for our observations could be that the latent heat released during the crystallization increases the local temperature resulting in proper crystallization and dendritic growth at larger distances from the nucleation core.

For all the films, circular waves of alternating lower and higher topographic features are observed on the continuous spherutlites. They display pseudo-periodic oscillations and start from the edge of the substrates propagating isotropically with (semi)circular fronts. Some of them are more ordered than the others, which we believe depends on the kinetics of the growth and the presence of material from other growing fronts on the particular location, as well as the presence of defects (e.g. particles, or mechanical indentations). These modulations have not been found on single-nucleus spherulites. As shown in the supplementary information (see figure S11), which images two single-nucleus spherulites at the center of the sample, with the original circular boundaries still visible, some of the fibers grow out of it forming continuous quartz, similarly to the spherulites at the edge (see figure S3). It is clear that the wave front carrying the oscillations started outside the region of the single-nucleus spherulites.

A possible reason for the wave formation is the mass transport that takes place during crystallization. The glass temperature of GeO_2 is about 700˚C and our annealing temperature is significantly above this[35]. Thus, we can assume the thin film is a supercooled liquid that is able to flow during annealing. Mass diffusion results in the accumulation (dendrites) at the growth front and depletion regions (around the dendrites) as it can be clearly observed in Figure4f). For the spherulitic growth, mass transport is not as prominent as during columnar growth but it is still present. As shown in Figure9 a)-b), first all the fiber growth ends at a trench (mass depletion), then the trenches are surrounded by a wall of material (mass accumulation). Moreover, on spherulites surrounded by amorphous

GeO_x, such as in Figure3d), Figure7c), height profiles show that material accumulate at the boundaries of spherulites resulting in a peak in height (see figure S12).

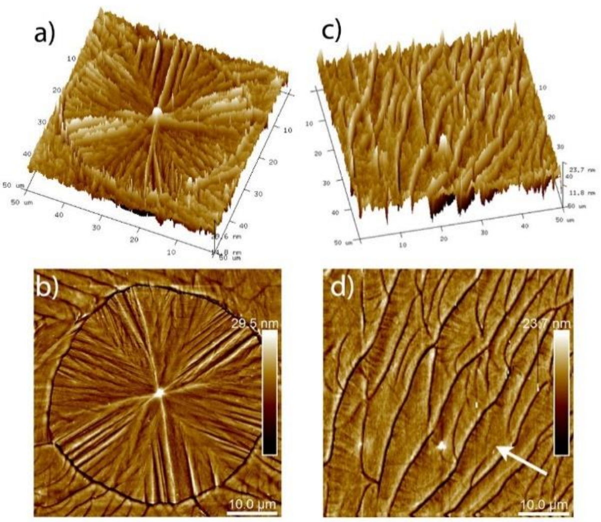

Figure 9 Quartz spherulites on *MgO* substrate with annealing temperature 830 C°. a)3-dimenSiOnal view of AFM image of b) shows a typical quartz single-nucleus spherulites: radial fibrous growth starting from the core. Note that the boundary of the domain is surrounded by a deep pitch, then followed by a high wall. c) 3-dimenSiOnal view of AFM image of d) shows the semi-periodic structure of quartz. Generally, each wave is composed of a relatively flat area with fibers, followed by a deep pitch and a high wall (depletion and the accumulation of material). The growth direction is shown by the arrow.

At the continuous quartz area, such as shown in Figure9, more clearly seen in the 3-dimensional view, the accumulation of the material forms high walls (the growth direction is shown by the arrow in the figure) and afterwards, fibers grow with flatter morphology. The presence of the trench suggests the depletion of the material. With the accumulation of the material, another period begins and so on.

Similar periodic structures caused by accumulation and depletion are also observed on the crystallizing of thin films of small molecules[36] and polymers[37][38]. It is worth to mention that, since the spherulitic growth is comparatively slow, it is likely that while the growth front is still propagating into the amorphous area, the crystallized part at the edge can recrystallize, which makes the whole process more complex.

5. **Conclusions**

We have successfully crystallized pure GeO_2 thin films into the quartz structure, on various substrates. Generally speaking, they share similar behaviors of spherulitic-to-crystalline growth: at relatively low annealing temperatures, the crystallization is spherulitic and with increasing temperatures, the growth transforms to dendritic growth at the growth front and, finally, to single crystalline growth. Lattice rotation, by which the lattice is rotating along the growth direction is observed on the spherulitic fibers and also the dendritic growth fibers but not on the single crystals.

Except for the thin films on $MgAl_2O_4$, nucleation is facilitated at the edge of the sample where half-circular spherulites with the nuclei at the sample edge are promoted, with the fibers from these spherulites growing together towards the center of the sample resulting in the crystallizing wave front sweeping from the sample edge to the center.

While on $MgAl_2O_4$ substrates, no preferential edge nucleation is found and rods-like small crystallites form at the amorphous area before attaching to the growing spherulites, which suggests the growth mechanism may be different than on other substrates.

For the thin films grown on *STO*, we found the *Sr* can react with the GeO_x and form a new compound $SrGeO_{3.3}O_{5.6}$, which is also spherulitic, at the interface between the substrate and the layer of crystallized quartz. A buffer layer of *TiO_2* can prevent this reaction and the whole film is crystallized into several macro domains, suggesting the growth rate is significantly accelerated compared to other substrates. Thin film of *GeO_2* are also crystallized on *LAO* with and without *TiO_2* buffer layer and the results are similar to those of on *TiO_2*-buffered *STO*.

6. Acknowledgements

This work is part of the research programme TOP-PUNT grant with project number 718.016002, which is financed by the Dutch Research Council (NWO).

7. Supplementary Information:

Please contact the authors to access the supplementary information (s.zhou@rug.nl)

8. References

[1] G.R. Johnson, History of the industrial production and technical development of single crystal cultured quartz, IEEE Int. Freq. Control Symp. 00 (2004) 35–45. https://doi.org/10.1109/FREQ.2004.1418426.

[2] F. Iwasaki, H. Iwasaki, Historical review of quartz crystal growth, J. Cryst. Growth. 237–239 (2002) 820–827. https://doi.org/10.1016/S0022-0248(01)02043-7.

[3] M. Tanaka, An overview of quartz MEMS devices, 2010 IEEE Int. Freq. Control Symp. FCS 2010. (2010) 162–167. https://doi.org/10.1109/FREQ.2010.5556352.

[4] F.P. Stratton, D.T. Chang, D.J. Kirby, R.J. Joyce, T.Y. Hsu, R.L. Kubena, Y.K. Yong, A MEMS-based quartz resonator technology for GHz applications, in: Proc. IEEE Int. Freq. Control Symp. Expo., IEEE, 2004: pp. 27–34. https://doi.org/10.1109/freq.2004.1418425.

[5] A. Carretero-Genevrier, M. Gich, L. Picas, J. Gazquez, G.L. Drisko, C. Boissiere, D. Grosso, J. Rodriguez-Carvajal, C. Sanchez, Soft-chemistry-based routes to epitaxial α-quartz thin films with tunable textures., Science. 340 (2013) 827–31. https://doi.org/10.1126/science.1232968.

[6] G.L. Drisko, A. Carretero-Genevrier, M. Gich, J. Gàzquez, D. Ferrah, D. Grosso, C. Boissière, J. Rodriguez-Carvajal, C. Sanchez, Water-induced phase separation forming macrostructured epitaxial quartz films on silicon, Adv. Funct. Mater. 24 (2014) 5494–5502. https://doi.org/10.1002/adfm.201401066.

[7] M. Gustafsson, F. Roccaforte, J. Keinonen, W. Bolse, L. Ziegeler, K.P. Lieb, Oxygen-activated epitaxial recrystallization of Li-implanted ?-SiO<inf>2</inf>, Phys. Rev. B - Condens. Matter Mater. Phys. 61 (2000) 3327–3332.

[8] F. Roccaforte, W. Bolse, K.P. Lieb, Solid phase epitaxial regrowth of ion beam-amorphized α-quartz, Appl. Phys. Lett. 73 (1998) 1349–1351. https://doi.org/10.1063/1.122159.

[9] J.F. Bertone, J. Cizeron, R.K. Wahi, J.K. Bosworth, V.L. Colvin, Hydrothermal synthesis of quartz nanocrystals, Nano Lett. 3 (2003) 655–659. https://doi.org/10.1021/nl025854r.

[10] X. Jiang, Y.B. Jiang, C.J. Brinker, Hydrothermal synthesis of monodisperse single-crystalline alpha-quartz nanospheres, Chem. Commun. 47 (2011) 7524–7526. https://doi.org/10.1039/c1cc11115a.

[11] L.M. Sochalski-Kolbus, H.-W. Wang, A.J. Rondinone, L.M. Anovitz, D.J. Wesolowski, P.S. Whitfield, Solvothermal Synthesis and Surface Chemistry To Control the Size and Morphology of Nanoquartz, Cryst. Growth Des. (2015) 151012150209002. https://doi.org/10.1021/acs.cgd.5b00882.

[12] P. Buckley, N. Hargreaves, S. Cooper, Nucleation of quartz under ambient conditions, Commun. Chem. 1 (2018) 49. https://doi.org/10.1038/s42004-018-0049-4.

[13] C.S. Marians, L.W. Hobbs, Network properties of crystalline polymorphs of silica, J. Non. Cryst. Solids. 124 (1990) 242–253. https://doi.org/10.1016/0022-3093(90)90269-R.

[14] E. Le Bourhis, Glass: Mechanics and Technology, 2014.

[15] A. Lignie, P. Armand, P. Papet, Growth of Piezoelectric Water-Free GeO$_2$ and SiO$_2$-Substituted GeO$_2$ Single-Crystals, Inorg. Chem. 50 (2011) 9311–9317.

[16] J.. Sarver, F.. Hummel, Alpha to Beta Transition, 43 (1959) 2303.

[17] V. V. Brazhkin, A.G. Lyapin, R.N. Voloshin, S. V. Popova, E. V. Tat’yanin, N.F. Borovikov, S.C. Bayliss, A. V. Sapelkin, Pressure-Induced Crossover between Diffusive and Displacive Mechanisms of Phase Transitions in Single-Crystalline [Formula presented], Phys. Rev. Lett. 90 (2003) 4. https://doi.org/10.1103/PhysRevLett.90.145503.

[18] P. Armand, S. Clément, D. Balitsky, A. Lignie, P. Papet, Large SiO2-substituted GeO2 single-crystals with the α-quartz structure, J. Cryst. Growth. 316 (2011) 153–157. https://doi.org/10.1016/j.jcrysgro.2010.12.030.

[19] A.G. Shtukenberg, Y.O. Punin, E. Gunn, B. Kahr, Spherulites, Chem. Rev. 112 (2012) 1805–1838. https://doi.org/10.1021/cr200297f.

[20] B. Crist, J.M. Schultz, Polymer spherulites: A critical review, Prog. Polym. Sci. 56 (2016) 1–63. https://doi.org/10.1016/j.progpolymsci.2015.11.006.

[21] S.-W. Park, J.-M. Choi, K.H. Lee, H.W. Yeom, S. Im, Y.K. Lee, Amorphous-to-Crystalline Phase Transformation of Thin Film Rubrene, J. Phys. Chem. B. 114 (2010) 5661–5665. https://doi.org/10.1021/jp910459p.

[22] P. Meakin, B. Jamtveit, Geological pattern formation by growth and dissolution in aqueous systems, Proc. R. Soc. A Math. Phys. Eng. Sci. 466 (2010) 659–694. https://doi.org/10.1098/rspa.2009.0189.

[23] G. Miehe, H. Graetsch, O.W. Flörke, Crystal structure and growth fabric of length-fast chalcedony, Phys. Chem. Miner. 10 (1984) 197–199. https://doi.org/10.1007/BF00309311.

[24] R. Hielscher, H. Schaeben, A novel pole figure inversion method: Specification of the MTEX algorithm, J. Appl. Crystallogr. 41 (2008) 1024–1037. https://doi.org/10.1107/S0021889808030112.

[25] A.M. Glazer, Confusion over the description of the quartz structure yet again, J. Appl. Crystallogr. 51 (2018) 915–918. https://doi.org/10.1107/S160057671800434X.

[26] V.Y. Kolosov, A.R. Thölén, Transmission electron microscopy studies of the specific structure of crystals formed by phase transition in iron oxide amorphous films, Acta Mater. 48 (2000) 1829–1840. https://doi.org/10.1016/S1359-6454(99)00471-1.

[27] B.J. Kooi, J.T.M. De Hosson, On the crystallization of thin films composed of Sb3.6Te with Ge for rewritable data storage, J. Appl. Phys. 95 (2004) 4714–4721. https://doi.org/10.1063/1.1690112.

[28] D. Savytskii, H. Jain, N. Tamura, V. Dierolf, Rotating lattice single crystal architecture on the surface of glass, Sci. Rep. 6 (2016). https://doi.org/10.1038/srep36449.

[29] M. Lucht, M. Lerche, H.C. Wille, Y. V. Shvyd'Ko, H.D. Rüter, E. Gerdau, P. Becker, Precise measurement of the lattice parameters of α-Al2O3 in the temperature range 4.5-250 K using the Mössbauer wavelength standard, J. Appl. Crystallogr. 36 (2003) 1075–1081. https://doi.org/10.1107/S0021889803011051.

[30] M.N. Gussev, K.J. Leonard, In situ SEM-EBSD analysis of plastic deformation mechanisms in neutron-irradiated austenitic steel, J. Nucl. Mater. 517 (2019) 45–56. https://doi.org/10.1016/j.jnucmat.2019.01.034.

[31] E. Demir, D. Raabe, Mechanical and microstructural single-crystal Bauschinger effects: Observation of reversible plasticity in copper during bending, Acta Mater. 58 (2010) 6055–6063. https://doi.org/10.1016/j.actamat.2010.07.023.

[32] J.H. Magill, D.J. Plazek, Physical Properties of Aromatic Hydrocarbons. II. Solidification Behavior of 1,3,5-Tri-α-Naphthylbenzene, J. Chem. Phys. 46 (1967) 3757–3769. https://doi.org/10.1063/1.1840448.

[33] A. Shtukenberg, E. Gunn, M. Gazzano, J. Freudenthal, E. Camp, R. Sours, E. Rosseeva, B. Kahr, Bernauer's bands, ChemPhysChem. 12 (2011) 1558–1571. https://doi.org/10.1002/cphc.201000963.

[34] L. Gránásy, T. Pusztai, G. Tegze, J.A. Warren, J.F. Douglas, Growth and form of spherulites, Phys. Rev. E - Stat. Nonlinear, Soft Matter Phys. 72 (2005) 1–15. https://doi.org/10.1103/PhysRevE.72.011605.

[35] P. Richet, GeO2 vs SiO2: Glass transitions and thermodynamic properties of polymorphs, Phys. Chem. Miner. 17 (1990) 79–88. https://doi.org/10.1007/BF00209228.

[36] J.S. Bangsund, T.R. Fielitz, T.J. Steiner, K. Shi, J.R. Van Sambeek, C.P. Clark, R.J. Holmes, Formation of aligned periodic patterns during the crystallization of organic semiconductor thin films, Nat. Mater. 18 (2019) 725–731. https://doi.org/10.1038/s41563-019-0379-3.

[37] J. Li, W. Peng, K. Chen, P. Wang, H.F. Chu, Y.F. Chen, D.N. Zheng, Growth and in situ high-pressure reflection high energy electron diffraction monitoring of oxide thin films, Sci. China Physics, Mech. Astron. 56 (2013) 2312–2326. https://doi.org/10.1007/s11433-013-5352-6.

[38] P. Poudel, S. Majumder, S. Chandran, H. Zhang, G. Reiter, Formation of Periodically Modulated Polymer Crystals, Macromolecules. 51 (2018) 6119–6126. https://doi.org/10.1021/acs.macromol.8b01366.